

Contents lists available at ScienceDirect

Journal of Sound and Vibration

journal homepage: www.elsevier.com/locate/jsvi





Noise influenced response movement in coupled oscillator arrays with multi-stability

Abdulrahman Alofi^a, Gizem Acar^b, Balakumar Balachandran^{a,*}

- ^a Department of Mechanical Engineering, University of Maryland, College Park, MD 20742, USA
- ^b Department of Mechanical Engineering, Stevens Institute of Technology, Hoboken, NJ 07030, USA

ARTICLE INFO

Keywords: Coupled oscillators White Gaussian noise Duffing oscillator Nonlinear dynamics Localization

ABSTRACT

In this work, the authors explore the influence of noise on the dynamics of coupled nonlinear oscillators. Numerical studies based on the Euler–Maruyama scheme and experimental studies with finite duration noise are undertaken to examine how the response can be moved from one response state to another by using noise addition to a harmonically forced system. In particular, jumps from a high amplitude state of each oscillator to a low amplitude state of each oscillator and the converse are demonstrated along with noise-influenced localizations. These events are found to occur in a region of multi-stability for the system, and the corresponding noise levels are reported. A method for recognizing how much noise is required to induce a change the system dynamics is developed by using the response basins of attraction. The findings of this work have implications for weakly coupled, nonlinear oscillator arrays and the manner in which noise can be used to influence energy localization and system dynamics in these systems.

1. Introduction

In small scale devices, systems vibrate at low amplitudes, wherein any small disturbance may affect the system dynamics [1]. In these systems, one usually encounters noise that is either derived from the surrounding environment or inherent to the system [2]. Even though the noise levels may be low, they can alter the system dynamics in a noticeable way. For instance, small fluctuations have been shown to move systems with metastable states escape from a local stable state [3]. Also, the presence of noise may induce a transition between a limit cycle and a fixed point of a system [4]. Moreover, noise may induce a period doubling cascade, resulting in chaos [5]. If not designed or addressed properly, not only will the performance of these systems be affected but there may be some undesirable consequences including system malfunction.

In recent years, researchers have investigated the influence of noise from a different perspective than done previously. Instead of building systems that are robust to noise, researchers have considered noise as a beneficial source of energy that could be exploited for enhancing system dynamics [6]. In particular, the phenomenon of stochastic resonance (SR) is mentioned. The presence of noise has been shown to enhance the stability of different system responses [7–9]. For an inverted pendulum, noise in combination with a vertical forcing has been shown to stabilize the unstable upright position [10]. In a different study, Chakraborty and Balachandran [11] showed through experimental and numerical studies that the addition of white Gaussian noise can help the system move from a no-contact state to a contact state, wherein the associated response is close to that of a period-doubled orbit. With a Duffing oscillator, Agarwal and Balachandran [12] showed that addition of noise can be used to move the system away from an aperiodic response, including the possibility to move the system from a chaotic motion to a fixed point of the unforced system.

E-mail address: balab@umd.edu (B. Balachandran).

^{*} Corresponding author.

Furthermore, noise has been used to reduce the hysteresis region (HR) or multi-stability region by moving the jump-up and the jump-down frequencies close to each other and reducing the HR [13].

While most of the studies in the area of mechanical systems have been to do with single and two degree of freedom systems, there have been a few studies related to coupled, oscillator array systems. In this regard, the influence of noise on intrinsic localized modes (ILMs) has been studied [14–18]. ILMs are spatially localized modes and time periodic solutions, which can occur in perfectly periodic lattices due to discreteness and nonlinearity in the considered system [19,20]. The concept of ILMs has been introduced to coupled oscillator arrays by Sato et al. [21,22]. Subsequently, different coupled oscillator models have been used to explore this phenomenon. The source of nonlinearity in these models has been geometrical nonlinearity [23,24], clearance nonlinearity [25], or nonlinear friction [26–28]. In these systems, each oscillator is in a motion state with either a high amplitude oscillation or a low amplitude oscillation, depending on the corresponding response mode. For example, a localized mode (LM) is the mode at which all of the oscillators vibrate in a state of low amplitude oscillations except one oscillator that vibrates in a state of high amplitude oscillation. The opposite to this mode is the anti-localized mode (ALM), wherein only one oscillator is oscillating in a state of low amplitude oscillation.

In a recent study, Papangelo et al. [29] investigated coupled oscillator arrays comprised of monostable oscillators, wherein the system can go into spatially localized responses. The degree of localization ranges from being in one oscillator to the extreme case, wherein all the oscillators vibrate at a high energy level. The energy state of the system can be studied with respect to different response branches, with each branch corresponding to a particular number of high amplitude oscillators. Ramakrishnan and Balachandran [16] investigated the influence of noise on localization in the form of ILMs. They found that noise can be used to strengthen as well as attenuate energy localizations in coupled oscillator arrays. Also, Perkins and Balachandran [17] carried out experimental and numerical investigations into coupled cantilever beam arrays. It was shown that localization can be destroyed, created, or even shifted to a different spatial location under the influence of noise. While the prior results have been illuminating, the focus of the prior studies has been mostly on the low energy, response branches. Further work is needed to understand if noise can be used to facilitate the movements between the other response branches, as seen for example in multi-oscillator systems (e.g., [29]), wherein jumps can occur in both upward and downward directions between response branches. As a first step to help with developing this understanding, a set of coupled, nonlinear oscillators are considered here and studied through experiments and numerical simulations.

In this work, three different sets of coupled oscillators are chosen for experimental examination. These sets include identical oscillators, nearly identical oscillators, and another one wherein one oscillator is a softening one while the other is a hardening one. Each set of oscillators is subjected to a combined excitation including a harmonic component and a noise component, and the frequency range of interest is based on the multi-stability region of the system. To the best of the authors' knowledge, the experiments with a softening, nonlinear oscillator coupled with a hardening, nonlinear oscillator is the first of its type to be conducted. The numerical studies are restricted to weakly coupled, identical nonlinear oscillators. From the results, it is gleaned that the influence of noise is highly dependent on the location within the considered multi-stability region. The rest of this paper is organized as follows. In Section 2, the experimental setup is presented. Following that, in Section 3, the system model is presented and discussed. In Section 4, the numerical scheme that is used for the simulations is shown. In Sections 6 and 7, the experimental and numerical results are presented and discussed, along with additional studies on coupled multi-oscillators arrays. Concluding remarks are presented to close the paper.

2. Experimental setup

In Fig. 1, the experimental setup that has been used to perform the study is shown. Inverted cantilever beams are used as building blocks for this model. The reduced order model of each beam with magnets can be chosen as a Duffing oscillator [12,13,30]. For that, a spring coupled set of metallic cantilever oscillators is secured to a base, which is connected to an electrodynamic shaker used to generate the excitation. The coupling springs are attached close to the fixed end of the beams, since the deflections in this region are smaller than the deflections near the beams' tips. This ensures linear behavior of the coupling springs. Permanent magnets are used to realize the nonlinear spring characteristics of each oscillator. For each cantilever oscillator, one of the magnets is located on top of the cantilever, while the other is fixed on a plate above the free end. An oscillator has softening characteristics when the gap between the pair of magnets is small. As the gap increases, the oscillator's response characteristics shift to hardening behavior. LabVIEW software is used to generate a combined excitation with harmonic and noise inputs. The excitation input is filtered by using a low pass filter so that only frequencies that are below a chosen cutoff frequency are allowed. The transverse deflections of the cantilevers in the excitation direction were measured by using strain gauges that are attached close to each cantilever's base. LabVIEW software is also used for data acquisition of the strain gauge signals. The experimental results are presented in Section 6.

3. System modeling

To compare with the experimental results obtained for coupled, identical nonlinear oscillators, a set of spring coupled, damped Duffing oscillators are considered. The corresponding schematic is shown in Fig. 2. In terms of the model, the interconnecting spring has a linear spring k_c and the system has free boundary conditions on either side. Each oscillator has a linear stiffness k_l and a cubic stiffness k_n . The governing equation of motions for the system are written as

$$m\frac{d^{2}x_{1}}{dt^{2}} + c\frac{dx_{1}}{dt} + k_{1}x_{1} + k_{nl}x_{1}^{3} + k_{c}(x_{1} - x_{2}) = f_{1}(t)$$

$$m\frac{d^{2}x_{2}}{dt^{2}} + c\frac{dx_{2}}{dt} + k_{l}x_{2} + k_{nl}x_{2}^{3} + k_{c}(x_{2} - x_{1}) = f_{2}(t)$$
(1)

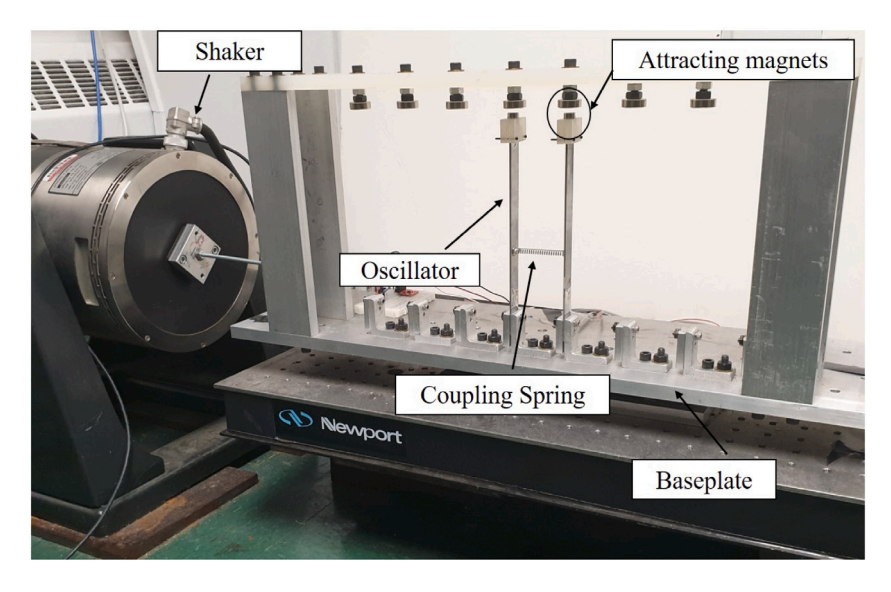


Fig. 1. Experimental setup of coupled oscillators. The beam oscillator close to the shaker is referred to as the first oscillator (OS1) and the other one is referred to as the second oscillator (OS2).

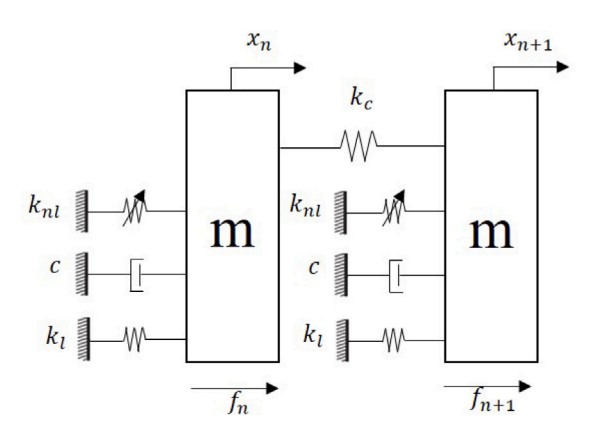


Fig. 2. Schematic of an array with two coupled oscillators. The oscillator on the left is referred to as the first oscillator (OS1) and the other one is referred to as the second oscillator (OS2).

Here, x_i is the displacement of the i th oscillator, m is the oscillator mass, c is the damping coefficient, and f_i is the force acting on the i th oscillator. This forcing is composed of a deterministic component in the form of a harmonic excitation and a stochastic input. In the stochastic input, which is in the form of white Gaussian noise $(\hat{\sigma} \dot{W}(t))$, $\hat{\sigma}$ is the noise intensity, and W(t) is the Wiener process. With the harmonic excitation given by $\hat{a}cos(\omega t)$, \hat{a} is the forcing amplitude and ω is the forcing frequency. Introducing the following parameters

$$\zeta = \frac{c}{2\sqrt{mk}}, \quad \omega_n^2 = \frac{k_l}{m}, \quad \beta = \frac{k_{nl}}{m}, \quad \alpha = \frac{k_c}{m}, \quad a = \frac{\hat{a}}{m}, \quad \text{and } \sigma = \frac{\hat{\sigma}}{m},$$

and assuming that the forcing is the same for the oscillators ($f_1 = f_2$), Eqs. (1) can be rewritten as follows:

$$\ddot{x}_1 + 2\zeta \omega_n \dot{x}_1 + \omega_n^2 x_1 + \beta x_1^3 + \alpha (x_1 - x_2) = a \cos(\omega t) + \sigma \dot{W}(t)$$

$$\ddot{x}_2 + 2\zeta \omega_n \dot{x}_2 + \omega_n^2 x_2 + \beta x_2^3 + \alpha (x_2 - x_1) = a \cos(\omega t) + \sigma \dot{W}(t)$$
(2)

Here, an overdot indicates the derivative with respect to time *t*. The parameters of the system are determined from the experimentally obtained frequency-response curves for the system shown in Fig. 1, as done in the group's prior studies (e.g., [13]).

4. Numerical scheme

Here, the scheme used for numerical simulations is described. As the derivative of Wiener process does not exist, Eqs. (2) are converted to a Langevin form, which has an incremental noise dW with zero mean and a standard deviation \sqrt{dt} . The result is

$$\begin{aligned} dz_1 &= z_2 dt \\ dz_2 &= (-2\zeta \omega_n z_2 - \omega_n^2 z_1 - \beta z_1^3 - \alpha (z_1 - z_3) + a \cos(\omega t)) dt + \sigma dW(t) \\ dz_3 &= z_4 dt \\ dz_4 &= (-2\zeta \omega_n z_4 - \omega_n^2 z_3 - \beta z_3^3 - \alpha (z_3 - z_1) + a \cos(\omega t)) dt + \sigma dW(t) \end{aligned} \tag{3}$$

The solution is obtained by numerically integrating equations (3) with the Euler–Maruyama scheme [31]. To obtain the localized modes, the authors have used the anti-continuous limit based method (e.g., [32]). With this method, the uncoupled system is considered first and the initial conditions are determined for the high amplitude and the low amplitude responses of an individual oscillator. Then, after introducing coupling and increasing the coupling strength gradually, and using the shooting method with an initial guess based on the response of the uncoupled system, periodic solutions for the coupled system are found.

5. Effects of coupling strength on system response

In this work, the authors are interested in the case with low coupling strength between the oscillators. For this case, the Van der Pol method is used to investigate the steady state solutions for different coupling values [33]. To begin with, the solution of Eq. (2) for a set of two coupled oscillators is assumed to have the following form:

$$x_i = u_i \cos \omega t - v_i \sin \omega t$$
 for $i = 1$ and 2 (4)

Here, u_i and v_i are unknown variables of time. The amplitude and phase of each oscillator are represented by $A_i = \sqrt{u_i^2 + v_i^2}$ and $\theta = v_i/u_i$, respectively. The system parameters are scaled by using a book keeping parameter ϵ as follows:

$$u_i, v_i : O(1), \quad \zeta, \beta, a : O(\epsilon) \quad \dot{u}_i, \dot{v}_i : O(\epsilon^2), \quad \ddot{u}_i, \ddot{v}_i : O(\epsilon^4)$$
 (5)

After substituting Eq. (4) into Eq. (2) with consideration of the scaling provided in Eq. (5), the governing equation for the approximate steady solutions can be found, up to the accuracy of $O(\epsilon^2)$, as follows:

$$2\omega\dot{u}_{1} = -2\zeta\omega\omega_{n0}u_{1} + \alpha v_{2} + (\omega^{2} - \omega_{n0}^{2} - \alpha)v_{1} - \frac{3}{4}\beta v_{1}(u_{1}^{2} + v_{1}^{2})$$

$$2\omega\dot{v}_{1} = -2\zeta\omega\omega_{n0}v_{1} - \alpha u_{2} + (-\omega^{2} + \omega_{n0}^{2} + \alpha)u_{1} + \frac{3}{4}\beta u_{1}(u_{1}^{2} + v_{1}^{2}) - a$$

$$2\omega\dot{u}_{2} = -2\zeta\omega\omega_{n0}u_{2} + \alpha v_{1} + (\omega^{2} - \omega_{n0}^{2} - \alpha)v_{2} - \frac{3}{4}\beta v_{2}(u_{2}^{2} + v_{2}^{2})$$

$$2\omega\dot{v}_{2} = -2\zeta\omega\omega_{n0}v_{2} - \alpha u_{1} + (-\omega^{2} + \omega_{n0}^{2} + \alpha)u_{2} + \frac{3}{4}\beta u_{2}(u_{2}^{2} + v_{2}^{2}) - a$$
(6)

To obtain the solutions for the different response branches from Eq. (6), the initial condition of (1,0) is first assigned for each oscillator based on the high amplitude or low amplitude assumptions. These solutions are then used in Auto software to continue the solution along each branch. For parameters similar to that of the first oscillator in the experimental arrangement described in Section 5, the solution of Eq. (6) is shown in Fig. 3(a)–(d) for different coupling parameters $\alpha=1$, $\alpha=3$, $\alpha=5$, and $\alpha=15$, respectively. For low coupling ($\alpha=1$), the ends of the two LMs are just before the ends for the unison modes, wherein all oscillators have the same response amplitudes. The unison modes are designated as high amplitude-high amplitude (high–high or H–H) or low amplitude-low amplitude (low–low or L–L) modes. As the coupling strength is increased, the amplitude gap between the LMs and the unison modes is found to increase. With further increase of the coupling strength, this gap is found to become larger with the inducement of a Hopf bifurcation as shown for $\alpha=15$. Here, the focus of the work has been on low coupling strength, in particular, $\alpha=1$ is considered. This coupling strength is considered to be relatively small. In Fig. 4, the bifurcation sets are shown in the $\alpha-\omega$ space. The solid thick lines are the boundary of the unison mode with the region for the high–high and the low–low modes illustrated by the thick black arrow. These modes are not affected by the increase in the coupling strength. The LMs are bounded by the solid light curves, which is illustrated by the light arrow. For a high coupling strength, a Hopf bifurcation is induced, and the loci of the Hopf instability points is shown by using the dotted–dashed curve.

6. Results and discussions

6.1. Array of similar oscillators: Experimental and numerical results

To begin with, the two oscillators are assumed to have identical properties. In the experiment, the two beam oscillators have been tuned to have an identical multi-stability frequency range ranging from $\omega = 33.81$ rad/s to 35.22 rad/s. This is illustrated by the responses observed for a quasi-static frequency sweep for the coupled oscillator, as shown in Fig. 5(a). The amplitude of each beam oscillator has been normalized by the corresponding maximum amplitude value. The multi-stability region (MR) is divided into six sections. The sections A, B, and C, which are on the upper branch, correspond to the left, middle and right regions, respectively. The corresponding sections on the lower branch are D, E, and F, respectively. Within this MR, localized modes (LMs) exist for the coupled oscillators; that is, modes in which one of the two beam oscillators is in the high branch while the other one is in the

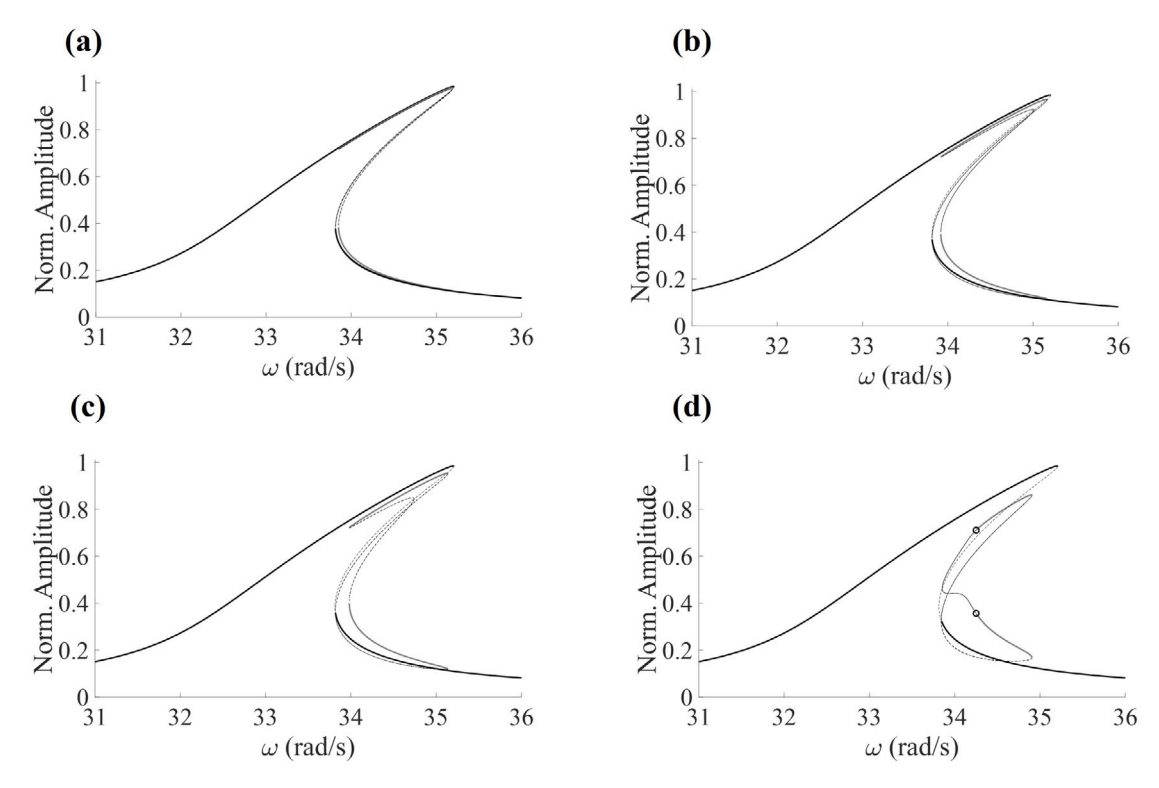


Fig. 3. Effects of coupling increase on the four response branches of the set of two coupled oscillators for the parameters obtained from the experiment in Fig. 5(a) for the first oscillator; that is $\zeta = 0.0079$, $\omega_n = 32.79$ rad/s, $\beta = 225.5$ N/kg m³, $\alpha = 1$ N/kg m and $\alpha = 17.95$ N/kg. The black curves correspond to the unison modes (high amplitude-high amplitude and low amplitude-low amplitude) and the gray curves correspond to the LMs. The coupling coefficient is as follows: (a) $\alpha = 1$, (b) $\alpha = 3$, (c) $\alpha = 5$, and (d) $\alpha = 15$.

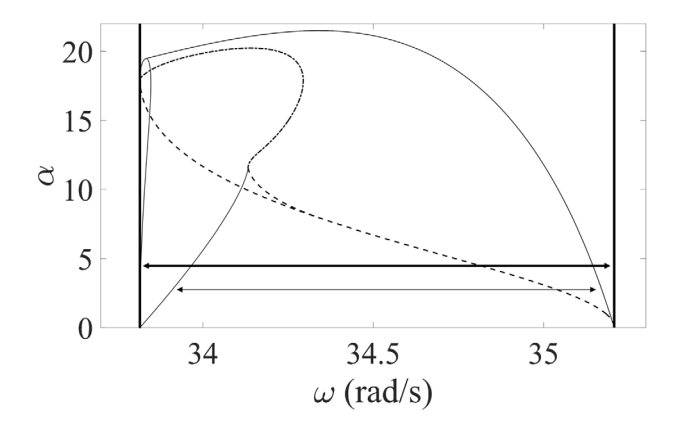


Fig. 4. Bifurcation sets in the (ω, α) plane for the system of two coupled oscillators with the parameters of Fig. 3. The thick black lines are the boundaries of the MR, the light black curves are the boundaries of the LMs, the dashed-dotted line is the loci of Hopf bifurcation points and the black dashed curves are unstable saddle points. The thick and light black arrows are used to represent the MR range and LM range, respectively.

low branch. The localized responses could not be found while performing the frequency sweep, and perturbations were applied to realize a localized mode. In the method used in the experiments, first, both oscillators are set to oscillate in a state of high amplitude oscillations in the middle of the MR. Next, a small disturbance is manually applied to one of the oscillators to move it from the high amplitude oscillation state to the low amplitude oscillation state. For numerical studies with the corresponding system, both of the two oscillators are assumed to have the properties of the first beam oscillator. The comparison between the experimental results and the numerical results of the first beam oscillator is shown in Fig. 5(b); good agreement is noted. Next, the influence of noise on system response is explored, with the possibility for jumps between different solution branches. In particular, harmonic excitations are considered with the excitation frequency being close to either end of the MR.

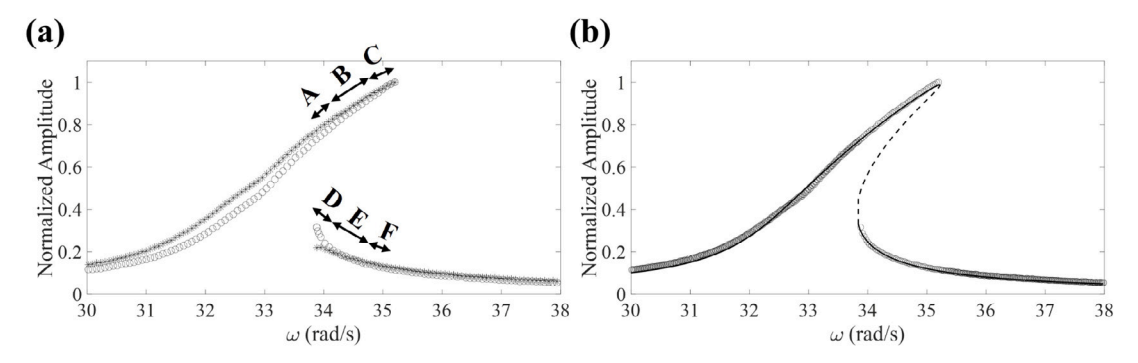


Fig. 5. Frequency responses of each of the two coupled oscillators: (a) Experimental results for the first oscillator (the dark curves in which points are shown with circles) and the second oscillator (the light curve in which points are shown with asterisk) of Fig. 1. (b) Comparison between experimental results (circles) with numerical results (solid line for the stable branch and dashed line for the unstable branch) of the first oscillator. While the experimental results are for the case of the coupled oscillators, the numerical results are for the uncoupled first oscillator. The corresponding system parameter values are as follow: ζ = 0.0079, $ω_n = 32.79 \text{ rad/s}$, $β = 225.5 \text{ N/kg m}^3$, α = 1 N/kg m and α = 17.95 N/kg.

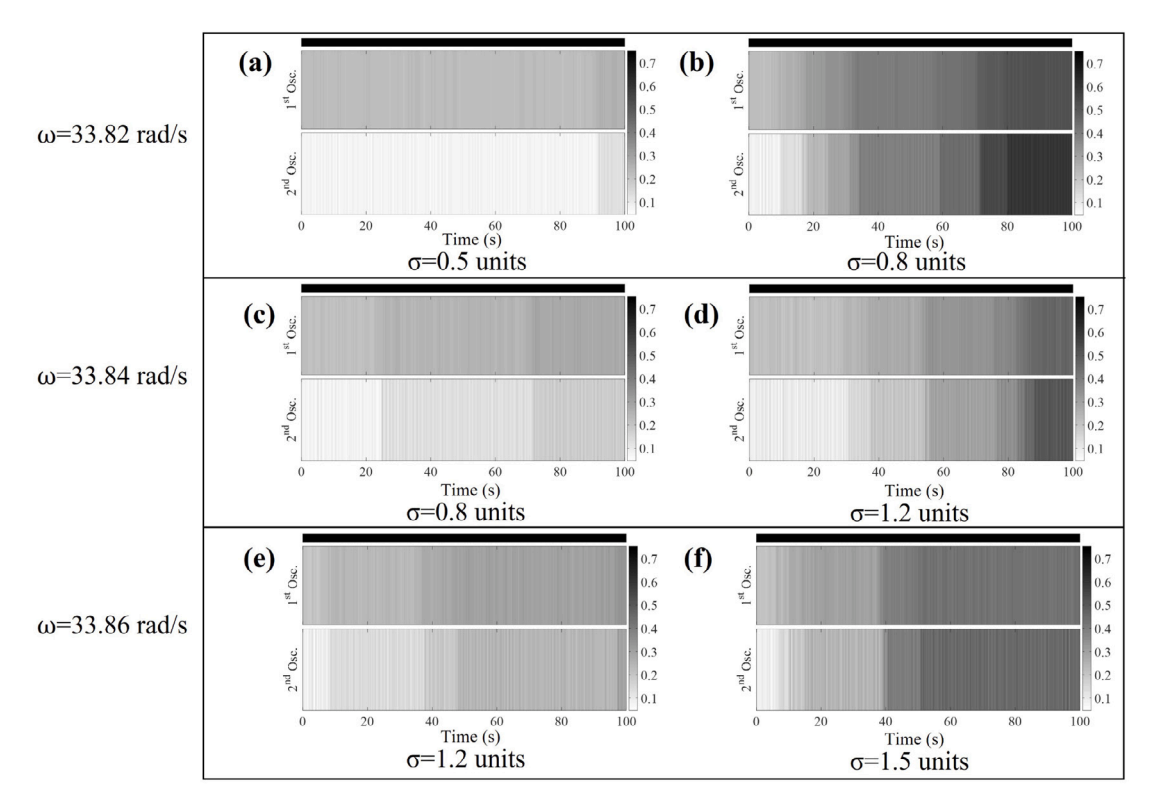


Fig. 6. Experimental results for the effects of finite duration noise in region D of Fig. 5. In this plot and all other similar plots, the RMS value of the displacements of the oscillators are shown, wherein the white region corresponds to the low amplitude state and the black region corresponds to the high amplitude state as shown in the vertical scale bar on the right. To determine the RMS values for this plot and others, the period of excitation is used, and this value is averaged over the different experiments considered for the chosen excitation frequency. In each time response plot, this RMS value is shown over the corresponding period. The horizontal black scale bar on the top is used to show the time windows over which noise is applied. In the present cases, noise has been applied over the whole interval shown. In each case, the RMS average over 12 experimental runs is plotted for each oscillator.

When the harmonic excitation frequency is set in region D of Fig. 5, the corresponding experimental results obtained are shown in Fig. 6. At each frequency, the experiment has been run twelve times over 100 s time windows for different noise intensities, starting from the low-low mode, a mode in which both beam oscillators have a low response amplitude when noise is not present. The root mean square (RMS) value over each period in each run is calculated for the whole interval. For the chosen noise input and excitation frequency, considering the 12 runs, the RMS value is then averaged and plotted. The averaged RMS value for each oscillator's response is represented in color over the corresponding time window with the white color corresponding to low amplitude

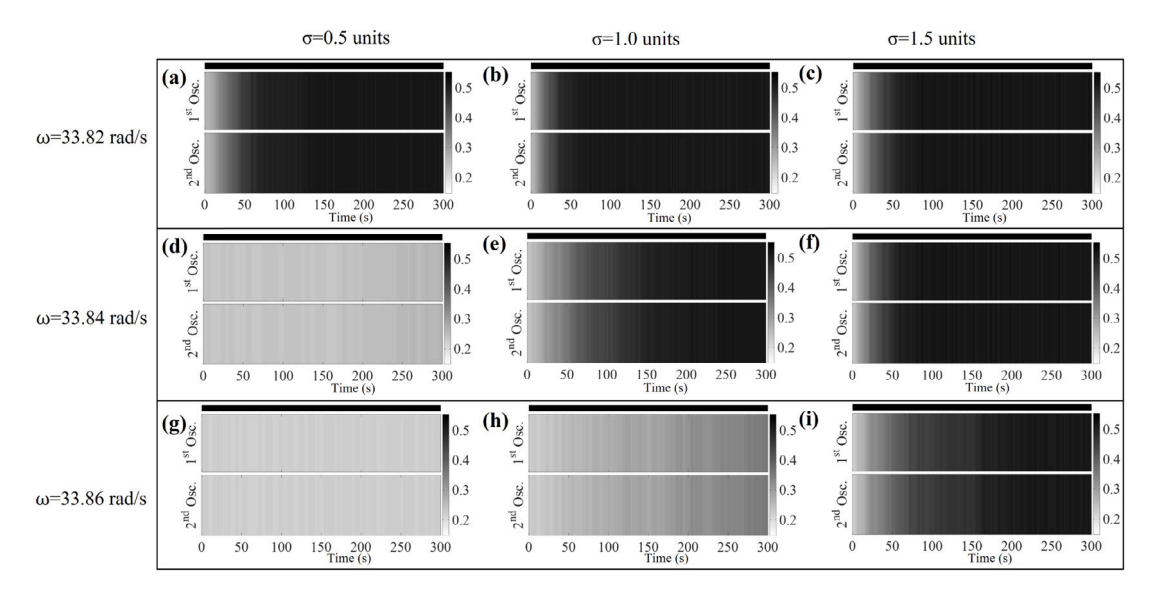


Fig. 7. Numerical results for the effects of finite duration noise in region D of Fig. 5. For each case, the RMS average over 50 numerical simulations is plotted for each oscillator.

oscillations and the black color corresponding to high amplitude oscillations. The horizontal black and white bar on the top is used to show the time windows over which noise is applied. In the present case, noise has been applied over the whole interval shown.

At the beginning of the experiments, the two oscillators are set to vibrate in the low-low mode in region D. Subsequently, noise has been applied and the responses of the two oscillators are found to move toward the high-high mode in region A, which is a mode in which each of the beam oscillators have a high amplitude response in the absence of noise. Close to the left boundary of region D (ω = 33.82 rad/s), for σ = 0.5 units, the oscillator responses jumped to the high-high mode eight times with the average time for transition being 77.5 s. In Fig. 6(a), the authors show the experimental results for this case. As can be seen, the color gradient for both oscillators tend to the black color at the end of the time interval. However, the responses still do not clearly reach a black color, indicating that jumps did not occur in all runs. At the same frequency value, when the noise intensity is increased to σ = 0.8 units, the responses in all of the cases were found to have moved to the high-high mode except in one occasion with the average time for transition being 50.5 s. The results are plotted in Fig. 6(b), and it is clearly evident that the response gradient color for both oscillators becomes black indicating in almost all of the runs, noise induced the jump. As the noise intensity is increased, it is observed that the time required to induce jumps is reduced. While the change in the response color gradient for σ = 0.5 units is limited in the first 50 s, there is a significant change for σ = 0.8 units.

Another experiment was conducted at $\omega=33.84$ rad/s for two different noise intensities, namely, $\sigma=0.8$ units and $\sigma=1.2$ units, and the results obtained are shown in Fig. 6(c) and (d), respectively. While for the noise intensity $of \sigma=0.8$ units, noise is found to have a pronounced impact on the response for $\omega=33.82$ rad/s, there is almost no impact on the response for $\omega=33.84$ rad/s. Only in two out of the 12 runs, the introduction of noise is found to induce jumps. However, for $\sigma=1.2$ units, the responses of the oscillators are found to jump to the high-high mode in 8 cases, indicating a noticeable effect of noise on the low-low mode. The experiments were also run further with $\omega=33.86$ rad/s for two noise intensities $\sigma=1.2$ units and $\sigma=1.5$ units. The corresponding results are shown in Fig. 6(e) and (f), respectively. For $\sigma=1.2$ units, as can be discerned from the response color gradient, only a small number of responses (4) moved into the high-high mode. On the other hand, for $\sigma=1.5$ units, in a relatively higher number of runs, a change in the system response dynamics (7 in this case) was observed.

The numerical results are obtained by solving Eq. (3) using Euler–Maruyama simulations. The average RMS value for the numerical simulation is obtained by considering the RMS average over 50 runs by using a different noise vector for each run. The results are plotted in Fig. 7. Similar ω values to those in the experiments were considered (ω = 33.82, 33.84, and 3.86 rad/s). For each ω value, three different noise intensities (σ = 0.5, 1.0, and 1.5 units)were used. In the case of the first frequency ω = 33.82 rad/s, successful jumps are observed to be induced for all noise intensities with the differences in the time required to induce that jump decreasing as the noise intensity was increased. For ω = 33.84 rad/s, a low noise intensity almost has no impact on the system dynamics, but the intermediate and high noise levels are found to be sufficient to induce a mode change with a transition time for the high noise level case being less than that for the medium level. For the last ω value (ω = 33.86 rad/s), again no effect on the response was observed when a low noise level was used. With the medium noise level, the change in responses occurred in less number of runs than those observed for the previous ω value. Only the high noise level was found to have a discernible impact on the low–low mode at this excitation frequency.

From the presented experimental and numerical results, one can note that the level of noise and the required time to move the system from the low-low mode to the high-high mode depend on the excitation frequency. Close to the left boundary of the MR

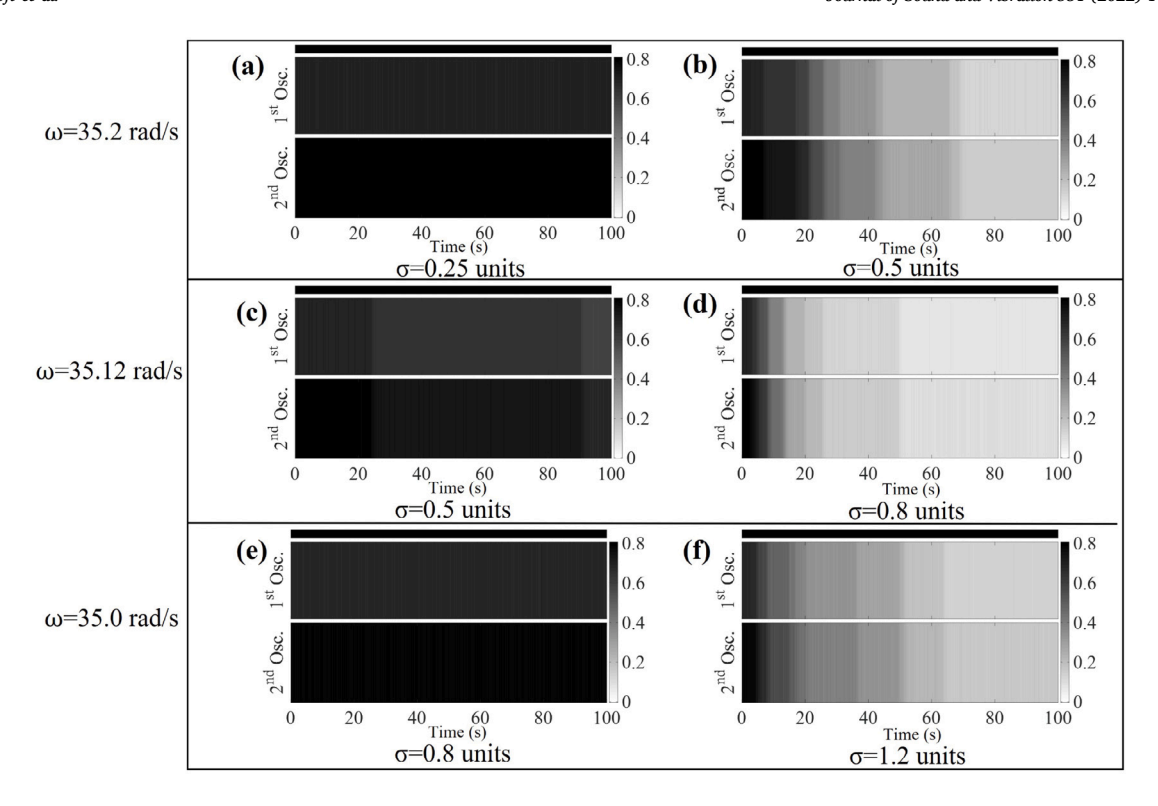


Fig. 8. Experimental results for the effects of finite duration noise in region C of Fig. 5. In each case, the RMS average over 12 experimental runs is plotted for each oscillator.

(boundary of region D), the low-low mode is sensitive to disturbances. Small disturbances are found to move the system response from the low-low mode to the high-high mode in a relatively small amount of time. When the harmonic excitation frequency is moved toward the center of the MR, the low-low mode is found to become robust to disturbances. High noise intensities are found to be needed to induce a response jump. The average time to induce a jump was found to increase as one moves toward the center of the MR and this time needed is found to decrease when the noise intensity is increased. It is clear that there is qualitative agreement amongst the experimental and numerical results. It is worth mentioning that when the system response is initiated in from the high-high mode, no change was observed in the system response dynamics under application of comparable noise intensities.

In Fig. 8, the authors have shown the experimental results obtained when the harmonic excitation frequency is close to right end of the MR. For this study, three different ω values are chosen and these values are 35.2, 35.12, and 35.0 rad/s. Similar to the previous experimental studies, for each parameter set, each test was run for twelve times in 100 s time windows and the average of the RMS value over the 12 runs is plotted. All runs are set to start from the high-high mode in region C to explore the possibility for changing the system dynamics to the low-low mode in region F.

At $\omega=35.2$ rad/s, the high-high mode was found to be quite sensitive for a low level noise disturbance. For a low noise intensity ($\sigma=0.25$ units), in eleven of the twelve cases, the system response collapsed to the low-low mode with the average transition time being 44.17 s. The associated dynamics is illustrated in Fig. 8(a). When the noise intensity is increased to $\sigma=0.5$ units, in all of the twelve cases, the system response collapsed within an average time of only 5.17 s, as illustrated in Fig. 8(b). Moving toward the center of the MR, the effects of two noise intensities are explored at $\omega=35.12$ rad/s. These intensities are $\sigma=0.5$ units and $\sigma=0.8$ units, and the corresponding results are depicted in Fig. 8(c) and (d), respectively. For $\sigma=0.5$ units, only in two of the twelve cases, the chosen noise input is found to induce a transition from the high-high mode to the low-low mode. By increasing the intensity further to $\sigma=0.8$ units, in all of the twelve cases, the response is found to collapse to the low-low mode within an average time of 14.67 s. At the last chosen ω value of ($\omega=35.0$ rad/s), the high-high mode is found to become robust to noise. When applying noise with $\sigma=0.8$ units, almost no effect on the response mode was observed. In none of the twelve cases, there was a change in the system dynamics, as shown in Fig. 8(e). For response jump downs to occur, a higher noise intensity is needed, as discernible from Fig. 8(f) for $\sigma=1.2$ units.

In Fig. 9, the average RMS value of the numerical simulation for 50 different noise vectors is plotted. There are differences between the excitation frequency values considered in the experiments and simulations, as there are differences in the manner in which the noise addition is carried out. In the experiments, bandlimited noise is applied while with the simulations, this restriction does not apply. Furthermore, in the experiments, apart from the spring coupling, there is coupling between the oscillators through the base. Due to these reasons, the authors only make qualitative comparisons. The numerical results are in good agreement with the experimental results. Close to edge of region C, small noise intensity is found to be sufficient to induce a jump from the high-high

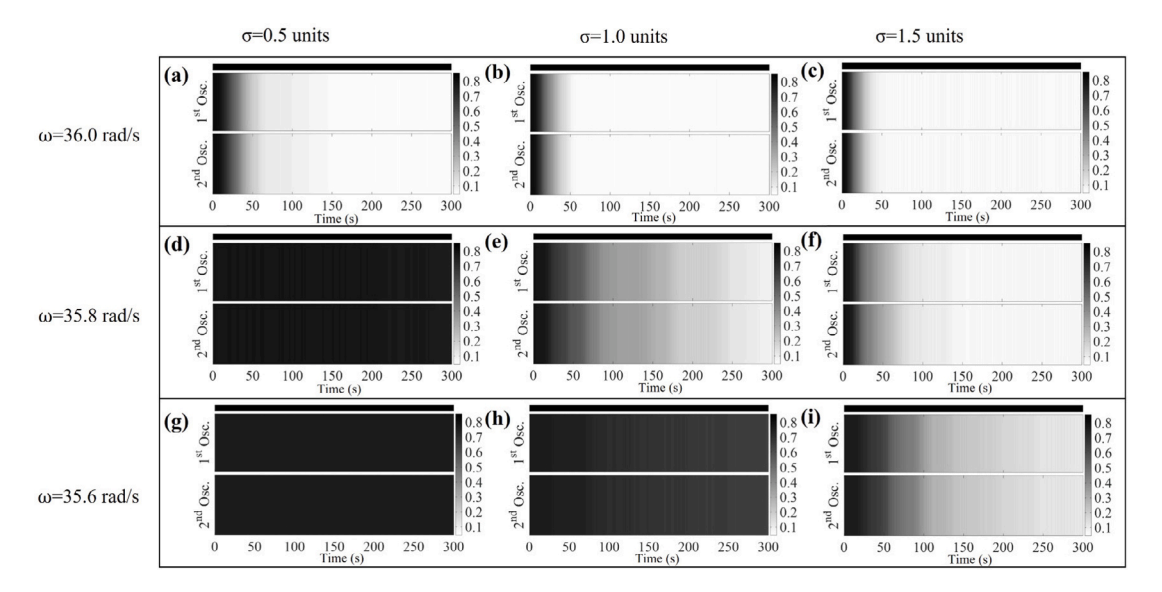


Fig. 9. Numerical results for the effects of noise in region C of Fig. 5. In each case, the RMS average over 50 experimental runs is plotted for each oscillator.

mode to the low-low mode. As one moves toward the center of region C, the required noise intensity to induce a jump is found to become higher. It is also noted that in the experiments and the simulations, no change in system response is found to occur when using comparable noise intensities as before to induce a jump from the low-low mode to the high-high mode.

Another remark is made with regard to the sensitivity of the response movement to the noise addition. It is found that when one is region C, a relatively low noise intensity is needed to realize a response movement or a jump down in this case to a low-low mode. However, at the end of region D, a relatively higher level of noise intensity is needed to realize a jump up from a low-low mode to a high-high mode. This can be explained by considering the basins of attraction of the responses of an uncoupled oscillator. It is known that the basin of attraction of the high amplitude response is smaller than that of the low amplitude response close to the jump down frequency. The relative ratio of the basins of attraction at the jump up frequency is different.

6.2. Arrays of near-identical and non-identical oscillators: Experimental results

Here, the findings from two different experimental studies are discussed. In one study, the experimental system consists of two nearly identical oscillators, both of which are of the hardening type. In the other study, the oscillators are different from each other, with one being a hardening oscillator and the other being a softening oscillator. The hardening and softening characteristics were realized by adjusting the spacing of magnets, shown in Fig. 1. These studies are expected to provide further insights into noise influenced dynamics of coupled oscillator arrays.

In the first case, the two beam oscillators are re-tuned so that a small mode localization window is realized in the system frequency response. A quasi-static frequency sweep is used to construct the frequency response curves first for the two coupled oscillators. These responses are shown in Fig. 10(a). The localization window of interest for the system is bracketed with two vertical lines (from ω = 34.2 rad/s to ω = 34.24 rad/s). In this window, each coupled oscillator's frequency response has two stable response branches, one with a relatively high amplitude and the other with a relatively low amplitude. One can have system modes with different response state combinations or modes, here, the high (OS1)-high (OS2) and high (OS1)-low (OS2) mode. At ω = 34.26 rad/s, the branches for the localized modes exist but do not appear, when one conducts a frequency sweep. First, movement of the system response to the high (OS1)-low (OS2) mode is considered. Close to the jump point, by adding noise with intensity σ = 0.8 for 14 s, the system response is steered to this LM, as shown in Fig. 10(b). To show that this mode is present, the noise addition is ceased after this 14 s of addition, and it is noted that this LM is present. To study a response movement to the high (OS1)-high (OS2) LM, noise addition is started at about 208 s and maintained for a longer duration of 190 s. The result is a movement to this LM of interest. Efforts to move the system response from a high (OS1)-high (OS2) LM to a high (OS1)-low (OS2) LM were not successful, and in these cases, the system response transitioned to a low (OS1)-low (OS2) mode. Overall, this set of experiments are illustrative of the use of finite duration noise to move the system response from one branch to another.

Similar qualitative results are also observed in the numerical studies. The oscillator in the arrays are assumed to have properties close to that of first oscillator in Fig. 10(a) with the natural frequencies being the only difference between the two oscillators. The analytical approximations for the responses of the uncoupled oscillators are shown in Fig. 10(c). Similar to the experiments, finite duration noise is used to induce response transition from the L–L response mode to the H–L response mode and then to the H–H response mode, as shown in Fig. 10(d).

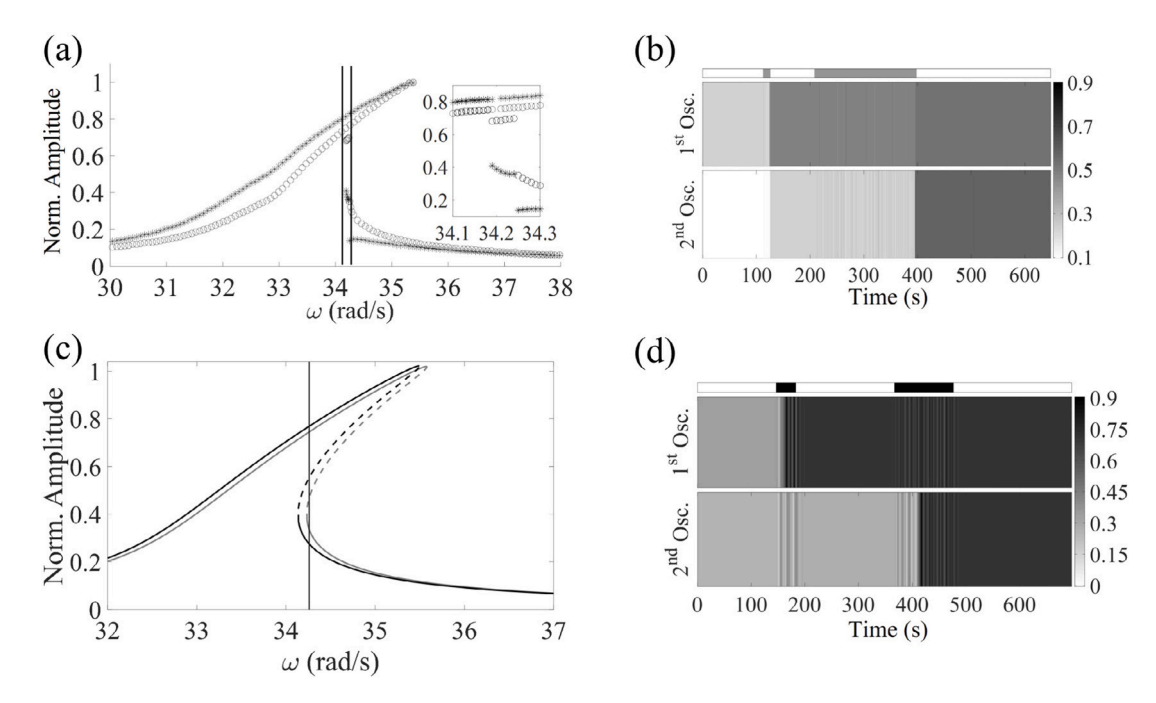


Fig. 10. Experimental results for a set of nearly identical oscillators: (a) Frequency response curves for the first oscillator (marked with dark circles) and the second oscillator (marked with lighter asterisks). The region of interest is demarcated with the two vertical black lines and an expanded view is provided in the inset. (b) Experimental RMS displacement values for both oscillators at ω = 34.26 rad/s and σ = 0.8 units, with the first oscillator response shown on the top and the second oscillator response shown in the bottom. The different shades used for the time responses correspond to different amplitude levels as explained in the text. The horizontal scale color bar is used on the top top into out the time windows (the dark regions) when noise addition is carried out. (c) Comparable analytical results for (a) with the gray curve for the first oscillator and the black curve for the second oscillator. The parameter values are ζ = 0.0075, $ω_{n01} = 33.25$ rad/s, $ω_{n02} = 33.15$ rad/s, β = 205 N/kg m³, α = 1 N/kg m and α = 18.0 N/kg. (d) RMS displacement values obtained in numerical studies with the influence of noise at ω = 34.26 rad/s.

For the second study, the second oscillator OS2 was not changed from the previous case and remained as a hardening oscillator, but the first oscillator OS1 is modified to be a softening oscillator as illustrated by the frequency response curves of Fig. 11(a). The region of interest is close to $\omega=34.87$ rad/s, wherein a vertical black line is shown. At $\omega=34.88$ rad/s, a jump down occurs in the response of the oscillator OS1 from the high amplitude branch to the low amplitude branch. At $\omega=34.86$ rad/s, a jump up occurs in the response of the oscillator OS2 from the low amplitude branch to the high amplitude branch. At $\omega=34.87$ rad/s, a branch of the high (OS1)-low (OS2) localized mode is initiated. Since this frequency is close to the jump down frequency of the first oscillator OS1, the localized mode is destroyed when noise is added to the coupled system. If one continues to apply noise to the system, a different localized mode is created, namely, the low (OS1)-high (OS2) mode. This noise influenced response movement is illustrated in Fig. 11(b). Again, this set of experimental results are illustrative of response movement that can be realized in coupled oscillator arrays with addition of noise of finite duration.

Similar results were obtained during numerical simulations. The properties of the first oscillator and the second oscillator are first obtained from the frequency response curve of Fig. 11(a). The analytical approximations for the responses of the uncoupled oscillators are shown in Fig. 11(c). The oscillator responses are first set to have a localization in the first oscillator. The application of noise results in a change in the spatial location of the localization to the second oscillator, as shown in Fig. 11(d).

6.3. Beyond an array of two coupled identical oscillators: Numerical results

Here, the authors extend their findings to multi-oscillator arrays. A set of 21 homogeneous oscillators with the same properties as the first oscillator OS1 in Fig. 5 are assumed to be coupled in a linear fashion with linear springs, so that each oscillator away from the boundary is coupled to its two adjacent neighbors. Each of the two boundary oscillators is only coupled on one side and free on the other side. Two cases of numerical simulations are considered. In the first case, a localized mode is considered at the excitation frequency $\omega = 33.87$ rad/s, which is near the left end of the multi-stability region. At this value, all of the oscillators have low amplitude responses except the middle one, which has a high amplitude response, as shown in Fig. 12(a). When noise is applied at $\sigma = 0.75$ units, the energy of the system is found to increase gradually with the oscillators on either side of the middle oscillator moving to their respective high amplitude states, as shown in Fig. 12(b). In the second case, an anti-localized mode is considered close to the right end of the multi-stability region; that is, $\omega = 35.17$ rad/s. In this anti-localization state, all of the oscillators have high amplitude responses except the middle one, which has a low amplitude response, as shown in Fig. 12(c). In Fig. 12(d), the

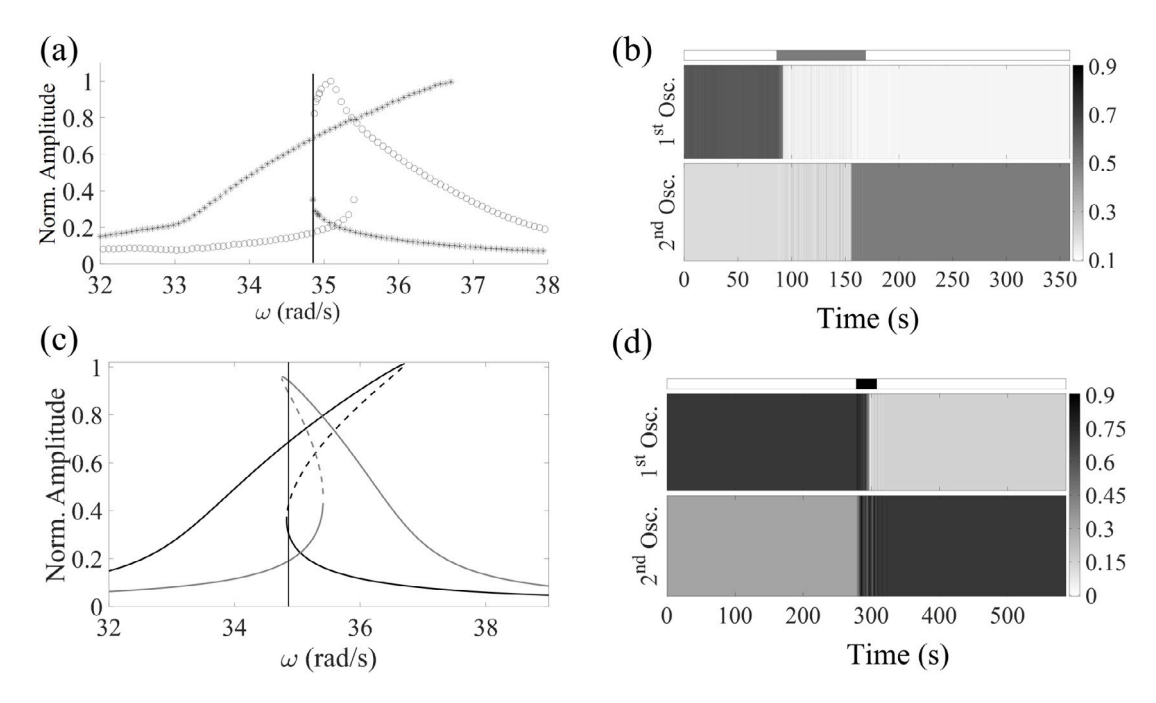


Fig. 11. Experimental results for a set of non-identical oscillators, with one being a hardening oscillator and the other being a softening oscillator. (a) Frequency response curves for the first oscillator (marked with dark circles) and the second oscillator (marked with lighter asterisks). The vertical black line goes through the jump down point for the first oscillator and jump up point for the second oscillator. (b) RMS displacement values for both oscillators at ω = 34.87 rad/s and σ = 1.0 units, with the first oscillator response shown on the top and the second oscillator response shown in the bottom. The different shades used for the time responses correspond to different amplitude levels as explained in the text. The horizontal scale color bar is used on the top to point out the time windows (the dark regions) when noise addition is carried out. (c) Comparable analytical results for (a) with the gray curve for the first oscillator and the black curve for the second oscillator. The parameter values are $ζ_1 = 0.00745$, $ω_{n01} = 36.22$ rad/s, $β_1 = -150$ N/kg m³, $α_1 = 1$ N/kg m and $a_1 = 18.0$ N/kg, $ζ_2 = 0.007175$, $ω_{n02} = 33.76$ rad/s, $β_2 = 270$ N/kg m³, $α_2 = 1$ N/kg m and $a_2 = 18.0$ N/kg. (d) RMS displacement values obtained in numerical studies with the influence of noise at ω = 34.87 rad/s.

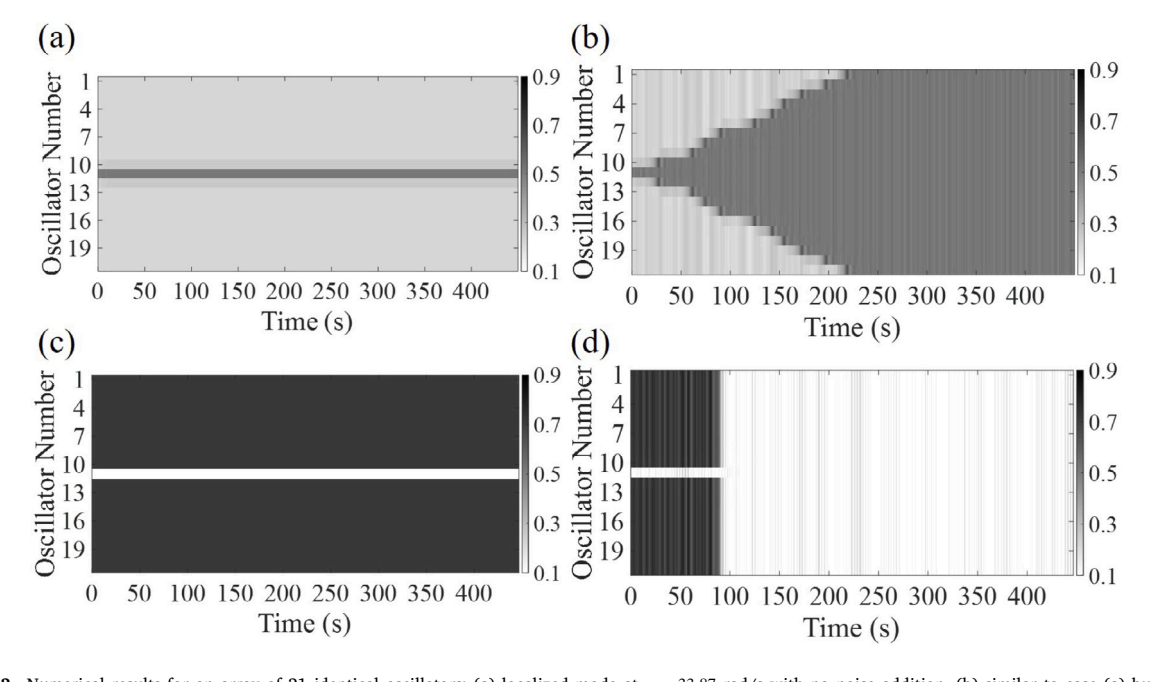


Fig. 12. Numerical results for an array of 21 identical oscillators: (a) localized mode at $\omega = 33.87$ rad/s with no noise addition, (b) similar to case (a) but with finite duration noise addition ($\sigma = 0.75$ units), (c) an anti-localization in the middle oscillator at $\omega = 35.17$ rad/s and no noise addition, and (d) similar to case (c) but with finite duration noise addition ($\sigma = 2.00$ units).

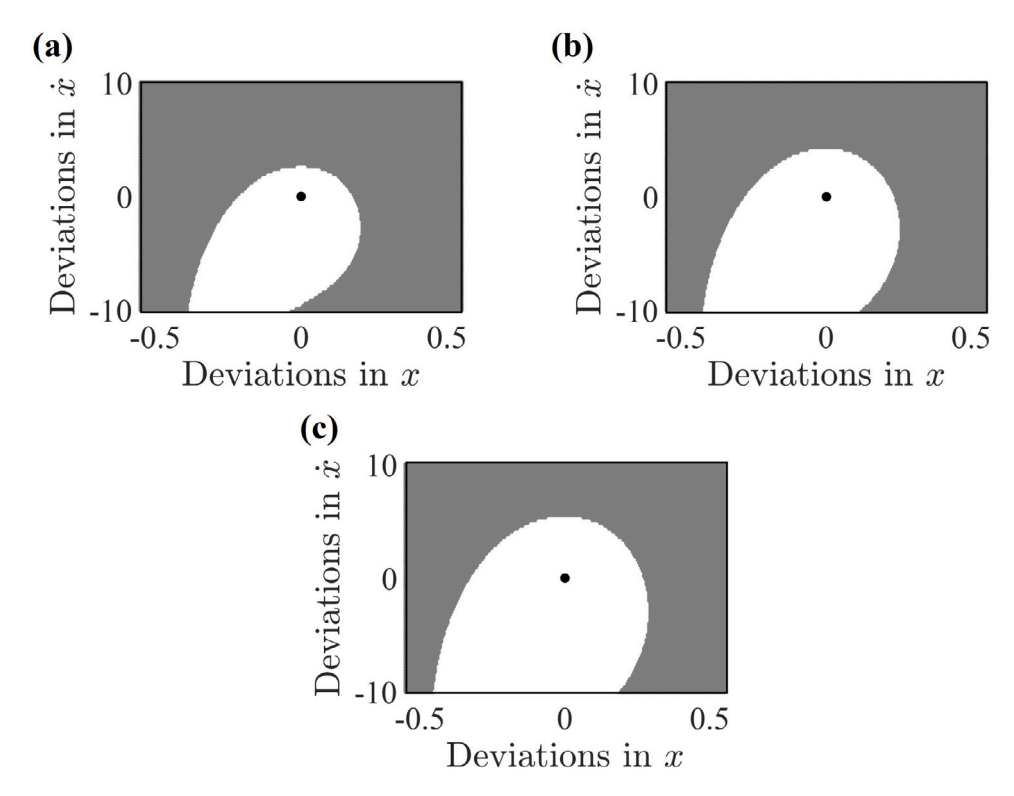


Fig. 13. Basin of attraction for the system near the left boundary of the MR starting from the L-L mode: (a) $\omega = 33.82$ rad/s, (b) $\omega = 33.84$ rad/s, and (c) $\omega = 33.86$ rad/s.

result is shown when noise is added with an intensity of $\sigma = 2.00$ units. All of oscillators with high amplitude responses move to their respective low amplitude states at the same time.

It is noted that the effects of noise on multi-oscillator arrays with more than two identical oscillators are similar to those noted with an array of two coupled, identical oscillators. This observation was also made in another recent study of the group [34]. On the left boundary of the system's multi-stability region in the frequency response, the oscillators tend to move to the high amplitude responses. Finite duration noise can be used to move all of the oscillators to a high amplitude state. However, at the right boundary of the multi-stability region of the frequency response, the oscillators tend to move to the low amplitude responses. A noise enabled response movement to a state of low amplitude can be accomplished.

7. Basins of attraction

To better understand the influence of disturbances on the system, the basins of attraction in region D are obtained and shown in Fig. 13. While the basins of attraction can be found for a four-dimensional system such as those considered here for two coupled oscillators, one often looks at a two-dimensional basin projection. The procedure used here to obtain this two-dimensional view is similar to the one used in the work of Ikeda et al. [33]. To find the basins, the initial conditions for a mode of interest (L–L, H–L, L–H, and H–H) is selected as the starting point for the numerical integration of the governing equations by using the ode45 solver in Matlab [35]. Next, a grid of 250*250 with (0,0) as the center point (black point in Fig. 13) is defined as a disturbance for the system. At the (0,0) point, no disturbance or deviation has been applied. For any other point, the first or x value is added to each displacement state $(x_1$ and $x_2)$ and the second or x value is added to each velocity state $(x_1$ and x_2) to represent deviations from the initial state of the system. System (2) is then solved for two oscillators for each point and the solution is traced after reaching the steady state solutions. Depending on the final state, each point is colored with either gray color (H–H) or white color (L–L).

In Fig. 13(a)–(c), the basins of attraction corresponding to region C are shown for the three previously considered ω values; that is, $\omega = 33.82$, 33,84, and 33.86 rad/s. The initial state for the system is in the L–L mode, and it is represented by the black point and this is the state at which no deviations have been applied. For $\omega = 33.82$ rad/s, when small deviations are applied, the system response is found to return to the original state of the L–L mode, and this falls within the white region. However, if the deviation is relatively large, the response no longer returns to the L–L mode but is drawn to the H–H mode. This falls within the gray region. When one moves toward the center of region C, the white region is found to expand further and the black dot is found to move more inside of the L–L mode, as shown in Fig. 13(b) and (c). The previous results might give an indication for what to expect in the response change after application of noise to the coupled oscillator arrays. For ω values close to the edge of region C, the L–L

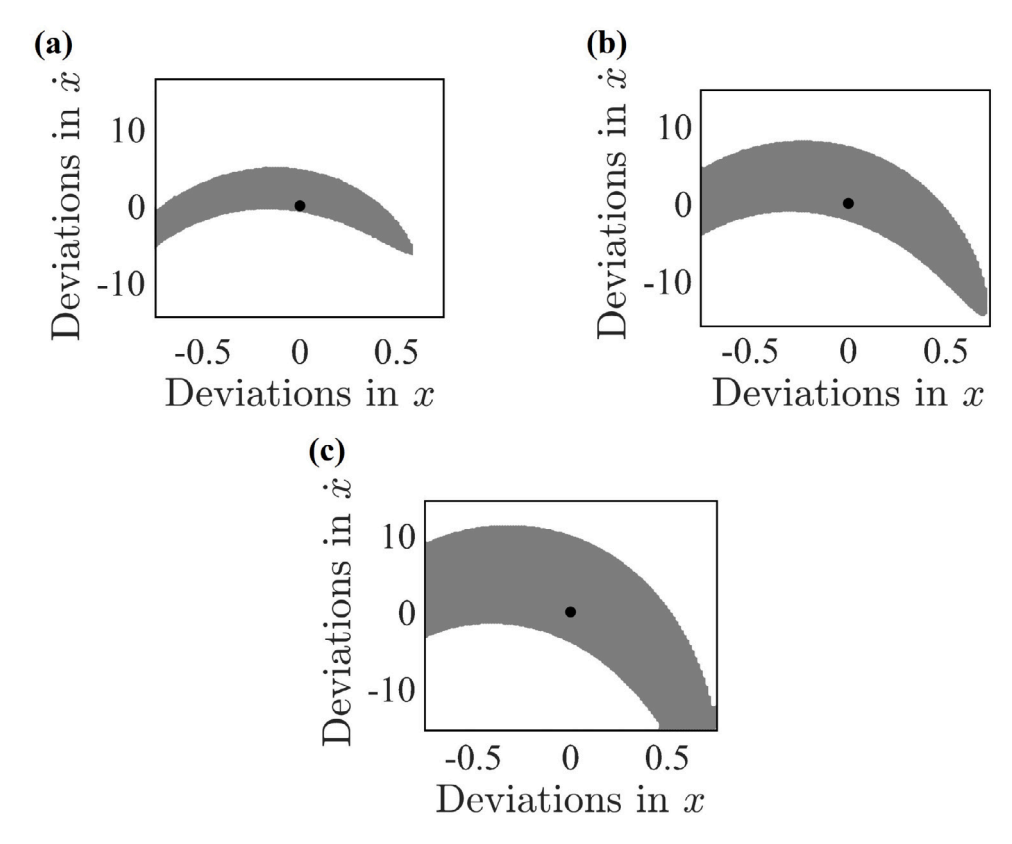


Fig. 14. Basins of attraction for the system near the right boundary of the MR starting from the H–H mode: (a) $\omega = 35.2$ rad/s, (b) $\omega = 35.12$ rad/s, and (c) $\omega = 35.0$ rad/s.

mode region is small in size indicating how sensitive this mode is to a noise disturbance. As a result, small disturbances might be enough to move the response mode into the H–H response mode. As one moves toward the center, the white region expands in size and higher noise intensities would be needed to induce a change in the system dynamics.

For region C, the following three ω values are considered: 35.2, 35.12, and 35.0 rad/s. The basins of attraction for this region are shown in Fig. 14(a)–(c). For ω = 35.2 rad/s, the H–H mode has a small basin that is shown as a small gray stripe in Fig. 14(a). When one moves toward the center of the MR region, the gray area expands in size as shown in Fig. 14(b) and (c). These plots might be used to understand how robust the H–H mode is to a disturbance in this region. When the gray area is small in size, it is expected that the H–H mode is vulnerable to a disturbance and the system response can be changed with a low intensity disturbance. However, as one moves toward the center, the gray region is found to expand in size, and high noise intensities are needed to alter the system dynamics. In the considered basin sets, there is no presence of basins of the localized mode responses. As a result, for the chosen initial conditions, it is less likely that one will obtain localized modes by subjecting the system to a noise addition.

8. Conclusion

In this work, the authors have shown how finite duration noise can be used to move the response of a harmonically excited oscillator array from one state to another. Particular attention was paid to the frequency region in which the system has a multistability response. As a basic setup to explore, the authors started with two spring coupled, nonlinear oscillators and showed through experiments that this response movement is possible from low amplitude states to high amplitude states and vice versa, depending on the excitation frequency relative to the multi-stability region. As noted previously, the experimental results obtained with a combination of hardening and softening oscillators is the first of its type. The experimental findings are also supported by the numerical results obtained with Euler–Maruyama simulations. The extension of the numerical studies to a high number of oscillators (more than 10) also brings forth the promise of using noise to engineer response movement in harmonically forced, coupled oscillator arrays. The studies with the high number of oscillators also confirm that a subset of his system can be used to capture the localization phenomenon, as also discussed in the context of circular oscillator arrays (e.g., [34]). For coupled oscillator systems, the results on the basins of attraction can be used as a tool to predict the behavior of the system dynamics under the influence of noise.

CRediT authorship contribution statement

Abdulrahman Alofi: Conceptualization, Methodology, Software, Validation, Investigation, Writing – original draft, Writing – review and editing. **Gizem Acar:** Methodology, Investigation. **Balakumar Balachandran:** Conceptualization, Methodology, Investigation, Writing – review and editing, Project administration, Funding acquisition.

Declaration of competing interest

The authors declare that they have no known competing financial interests or personal relationships that could have appeared to influence the work reported in this paper.

Acknowledgments

The authors would like to appreciate the support received for this work through National Science Foundation NSF, USA Grant No. CMMI1760366. Also, the first author acknowledges the fellowship received from King Fahd University of Petroleum and Minerals, Saudi Arabia.

Funding

Funding was received from the U.S. National Science Foundation.

References

- [1] J.R. Vig, Y. Kim, Noise in microelectromechanical system resonators, IEEE Trans. Ultrason. Ferroelectr. Freq. Control 46 (6) (1999) 1558–1565, http://dx.doi.org/10.1109/58.808881.
- [2] F. Mohd-Yasin, D. Nagel, C. Korman, Noise in MEMS, Meas. Sci. Technol. 21 (1) (2009) 012001, http://dx.doi.org/10.1088/0957-0233/21/1/012001.
- [3] P. Hanggi, Escape from a metastable state, J. Stat. Phys. 42 (1-2) (1986) 105-148, http://dx.doi.org/10.1007/BF01010843.
- [4] I. L'Heureux, R. Kapral, White noise induced transitions between a limit cycle and a fixed point, Phys. Lett. A 136 (9) (1989) 472–476, http://dx.doi.org/10.1016/0375-9601(89)90298-3.
- [5] J. Gao, S. Hwang, J. Liu, When can noise induce chaos? Phys. Rev. Lett. 82 (6) (1999) 1132, http://dx.doi.org/10.1103/PhysRevLett.82.1132.
- [6] F. Chapeau-Blondeau, Stochastic resonance and the benefit of noise in nonlinear systems, in: Noise, Oscillators and Algebraic Randomness, Springer, 2000, pp. 137–155, http://dx.doi.org/10.1007/3-540-45463-2_7.
- [7] N. Agudov, B. Spagnolo, Noise-enhanced stability of periodically driven metastable states, Phys. Rev. E 64 (3) (2001) 035102, http://dx.doi.org/10.1103/PhysRevE.64.035102.
- [8] R. Mantegna, B. Spagnolo, Noise enhanced stability in an unstable system, Phys. Rev. Lett. 76 (4) (1996) 563, http://dx.doi.org/10.1103/PhysRevLett.76.
- [9] A.A. Dubkov, N. Agudov, B. Spagnolo, Noise-enhanced stability in fluctuating metastable states, Phys. Rev. E 69 (6) (2004) 061103, http://dx.doi.org/10. 1103/PhysRevE.69.061103.
- [10] E. Perkins, B. Balachandran, Noise-influenced dynamics of a vertically excited pendulum, in: ASME 2013 International Design Engineering Technical Conferences and Computers and Information in Engineering Conference, American Society of Mechanical Engineers, Portland, Oregon, USA, 2013, http://dx.doi.org/10.1115/DETC2013-12336, V07BT10A025.
- [11] I. Chakraborty, B. Balachandran, Noise influenced elastic cantilever dynamics with nonlinear tip interaction forces, Nonlinear Dynam. 66 (3) (2011) 427–439, http://dx.doi.org/10.1007/s11071-011-0034-2.
- [12] V. Agarwal, B. Balachandran, Noise-influenced response of Duffing oscillator, in: ASME 2015 International Mechanical Engineering Congress and Exposition, American Society of Mechanical Engineers, Houston, Texas, USA, 2015, http://dx.doi.org/10.1115/IMECE2015-51620, V04BT04A019.
- [13] V. Agarwal, X. Zheng, B. Balachandran, Influence of noise on frequency responses of softening Duffing oscillators, Phys. Lett. A 382 (46) (2018) 3355–3364, http://dx.doi.org/10.1016/j.physleta.2018.09.008.
- [14] E. Perkins, M. Kimura, T. Hikihara, B. Balachandran, Effects of noise on symmetric intrinsic localized modes, Nonlinear Dynam. 85 (1) (2016) 333–341, http://dx.doi.org/10.1007/s11071-016-2688-2.
- [15] S. Ramakrishnan, B. Balachandran, Intrinsic localized modes in micro-scale oscillator arrays subjected to deterministic excitation and white noise, in: IUTAM Symposium on Multi-Functional Material Structures and Systems, Springer, 2010, pp. 325–334, http://dx.doi.org/10.1007/978-90-481-3771-8_33.
- [16] S. Ramakrishnan, B. Balachandran, Energy localization and white noise-induced enhancement of response in a micro-scale oscillator array, Nonlinear Dynam. 62 (1–2) (2010) 1–16, http://dx.doi.org/10.1007/s11071-010-9694-6.
- [17] E. Perkins, B. Balachandran, Noise-enhanced response of nonlinear oscillators, Procedia Iutam 5 (2012) 59–68, http://dx.doi.org/10.1016/j.piutam.2012. 06.009.
- [18] S. Ramakrishnan, B. Balachandran, Influence of noise on discrete breathers in nonlinearly coupled micro-oscillator arrays, in: IUTAM Symposium on Dynamics Modeling and Interaction Control in Virtual and Real Environments, Springer, 2011, pp. 247–254.
- [19] A. Sievers, S. Takeno, Intrinsic localized modes in anharmonic crystals, Phys. Rev. Lett. 61 (8) (1988) 970, http://dx.doi.org/10.1103/PhysRevLett.61.970.
- [20] D. Campbell, S. Flach, Y. Kivshar, et al., Localizing energy through nonlinearity and discreteness, Phys. Today 57 (1) (2004) 43–49, http://dx.doi.org/10. 1063/1.1650069.
- [21] M. Sato, B. Hubbard, A. Sievers, B. Ilic, D. Czaplewski, H. Craighead, Observation of locked intrinsic localized vibrational modes in a micromechanical oscillator array, Phys. Rev. Lett. 90 (4) (2003) 044102.
- [22] M. Sato, B. Hubbard, A. Sievers, Colloquium: Nonlinear energy localization and its manipulation in micromechanical oscillator arrays, Rev. Modern Phys. 78 (1) (2006) 137.
- [23] M. Didonna, M. Stender, A. Papangelo, F. Fontanela, M. Ciavarella, N. Hoffmann, Reconstruction of governing equations from vibration measurements for geometrically nonlinear systems, Lubricants 7 (8) (2019) 64.
- [24] A. Nitti, M. Stender, N. Hoffmann, A. Papangelo, Spatially localized vibrations in a rotor subjected to flutter, Nonlinear Dynam. 103 (1) (2021) 309-325.
- [25] B. Niedergesäß, A. Papangelo, A. Grolet, A. Vizzaccaro, F. Fontanela, L. Salles, A. Sievers, N. Hoffmann, Experimental observations of nonlinear vibration localization in a cyclic chain of weakly coupled nonlinear oscillators, J. Sound Vib. 497 (2021) 115952.

- [26] A. Papangelo, A. Grolet, L. Salles, N. Hoffmann, M. Ciavarella, Snaking bifurcations in a self-excited oscillator chain with cyclic symmetry, Commun. Nonlinear Sci. Numer. Simul. 44 (2017) 108–119.
- [27] A. Papangelo, N. Hoffmann, A. Grolet, M. Stender, M. Ciavarella, Multiple spatially localized dynamical states in friction-excited oscillator chains, J. Sound Vib. 417 (2018) 56–64.
- [28] I. Shiroky, A. Papangelo, N. Hoffmann, O. Gendelman, Nucleation and propagation of excitation fronts in self-excited systems, Physica D 401 (2020) 132176.
- [29] A. Papangelo, F. Fontanela, A. Grolet, M. Ciavarella, N. Hoffmann, Multistability and localization in forced cyclic symmetric structures modelled by weakly-coupled Duffing oscillators, J. Sound Vib. 440 (2019) 202–211, http://dx.doi.org/10.1016/j.jsv.2018.10.028.
- [30] Y. Jia, Review of nonlinear vibration energy harvesting: Duffing, bistability, parametric, stochastic and others, J. Intell. Mater. Syst. Struct. 31 (7) (2020) 921–944
- [31] D. Higham, An algorithmic introduction to numerical simulation of stochastic differential equations, SIAM Rev. 43 (3) (2001) 525–546, http://dx.doi.org/ 10.1137/S0036144500378302.
- [32] J. Marin, S. Aubry, Breathers in nonlinear lattices: numerical calculation from the anticontinuous limit, Nonlinearity 9 (6) (1996) 1501.
- [33] T. Ikeda, Y. Harata, K. Nishimura, Intrinsic localized modes of harmonic oscillations in nonlinear oscillator arrays, J. Comput. Nonlinear Dyn. 8 (4) (2013) 041009
- [34] B. Balachandran, T. Breunung, G. Acar, A. Alofi, J.A. Yorke, Coupled circular Duffing oscillator arrays under noise, Nonlinear Dynam. (2021).
- [35] MATLAB, 9.7.0.1190202 (R2019b), The MathWorks Inc., Natick, Massachusetts, 2018.